remote sensing

MDPI

Technical Note

Ship Wake Detection in a Single SAR Image via a Modified Low-Rank Constraint

Yanan Guan [1], Huaping Xu [1,*], Wei Li [2] and Chunsheng Li [1]

[1] School of Electronics and Information Engineering, Beihang University, Beijing 100191, China; guanyanan@buaa.edu.cn (Y.G.); lics@buaa.edu.cn (C.L.)
[2] Shanghai Institute of Satellite Engineering, Shanghai 200240, China; liwei20rth@139.com
* Correspondence: xuhuaping@buaa.edu.cn

Abstract: Ship wake detection stands as a pivotal task in marine environment monitoring. The main challenge in ship wake detection is to improve detection accuracy and mitigate false alarms. To address this challenge, a novel procedure for ship wake detection in a single SAR image is proposed in this study. Initially, an entropy distance similarity criterion is designed to measure nonlocal image patch similarity. Based on the proposed criterion, a low-rank and sparse decomposition method is modified using nonlocal similar patch matrix construction to separate the sparse wake. Subsequently, a field-of-experts (FOE) model is introduced to generate a series of multi-view wake feature maps, which are fused to construct an enhanced feature map. The sparse wake is further enhanced in the Radon domain with the enhanced feature map. The experimental results demonstrate the effectiveness of the proposed method on real SAR ship wake images.

Keywords: ship wake detection; Radon; SAR image; sea clutter; low rank; feature enhancement

Citation: Guan, Y.; Xu, H.; Li, W.; Li, C. Ship Wake Detection in a Single SAR Image via a Modified Low-Rank Constraint. *Remote Sens.* **2024**, *16*, 3487. https://doi.org/10.3390/rs16183487

Academic Editors: Dusan Gleich and Stefano Tebaldini

Received: 14 July 2024
Revised: 29 August 2024
Accepted: 13 September 2024
Published: 20 September 2024

1. Introduction

As an active Earth observation system, synthetic aperture radar (SAR) facilitates all-weather and all-day surveillance with extensive coverage [1,2]. The acquisition of high-resolution SAR images has attracted significant attention for target detection, particularly in oceanic applications, where it serves as an effective tool [3]. When a moving ship sails on a rough sea surface, the generated wake patterns appear on the surface in large sizes. The visible appearances of the wake patterns are mainly associated with the ship's parameters, such as the speed, the ship hull size, and so on [4–6]. These moving-ship parameters can also be inverted through analysis of the ship wake captured in an SAR image [3]. Thus, detecting ship wake patterns in SAR images plays a crucial role in marine environment monitoring [7,8].

Ship wake patterns are generally modeled as linear structures [9,10], given that they have typical linear characteristics and appear as bright or dark lines in SAR images. As a result, the detection of a ship's wake is formulated using lines identified against the sea clutter background in SAR images in the existing literature [7–13]. There is significant utilization of the Radon transform (RT) and Hough transform (HT) for detecting these linear wake structures, benefiting from their superior line recognition abilities [9,13]. The RT is used to calculate the image pixel accumulation in various directions and then map lines in image domains into peak points in the Radon domain. Compared with the HT, the RT has the capability of canceling out the impact of noise fluctuations by integrating image pixels in specific directions [14]. This principle makes the RT more prevalent in wake detection in SAR images [15,16]. When employing the RT for wake detection, the bright (dark) lines in the SAR image domain are transformed into bright (dark) peak points in the Radon domain. These distinctive peak points of wake signatures can be identified and extracted against an appropriate threshold [17]. Murphy adopted the RT to detect the linear characteristics of wakes in SAR images for the first time and demonstrated that the

linear features of wakes are enhanced during the process of image pixel integration. The enhanced features produced good detection results [18]. Meanwhile, the study also pointed out that more investigations are required for wake patterns in complex environments. Wake patterns are disturbances of the sea surface that generate interactions with sea gravity and capillary waves. Then, the roughness of the sea surface is changed, and wakes can appear in SAR images based on the mechanism of wake pattern SAR imaging. Wake patterns can be considered a superposition above the sea's surface. The observability of wake patterns is flexibly influenced by complex image backgrounds. Heavy sea clutter at a high sea wave height can cause high false-alarm probability and even conceal wake patterns [10]. It is a challenge to obtain great performance against these complex backgrounds in ship wake detection in SAR images. Thus, these RT-based wake detection methods are mainly promoted by improving the wake's signal-to-noise ratio (SNR), which aims to reduce the influence of these backgrounds.

Combining image preprocessing techniques with the Radon transform is a common strategy [9,10]. High-pass filters and Wiener filters are used in the image and Radon domains, respectively, in order to suppress sea clutter and reduce the appearance rate of false ship wakes [18]. The localized Radon transform proposed by Copeland et al. uses a series of local windows to isolate and locate peak points to reduce some false alarms [12]. The wavelet transform based on an orthogonal basis was developed to generate multi-scale high-pass images [19], and the edges of wakes can be enhanced by correlating the high-pass image modulus, thus reducing false points in the Radon domain. Stochastic matched filtering was combined with the RT to enhance wake shapes in the frequency domain; the wake showed X-shaped features, and the RT was still used to detect the lines of X-shaped features [20]. In addition, a few ship wake detection methods have been developed based on deep learning [10]. However, most of them are data-driven and have a high dependence on large-scale wake datasets, which are difficult to obtain [10,21]. The idea of compressed sensing has recently been introduced to tackle the wake detection problem. The key is to separate wake patterns from the image background, following which the separated wake patterns are still detected using the RT. A sparse dictionary for ship wake textures and a sparse dictionary for sea clutter textures were designed by Yang et al. [22], which adopted morphological component analysis to extract the wake components, and RT was adopted to identify the wake. The generalized minimax concave (GMC) [15] function was introduced as another sparse regularization approach to enhance the linear features of the wake and reduce false alarms in the Radon domain.

Inspired by sparse regularization, approaches based on low-rank plus sparse decomposition (LRSD) have been successfully utilized for the task of wake detection in a single SAR image [23,24]. Low rank is a prior characteristic of SAR images and represents a high correlation among images [25]. Based on this, an observed SAR image can be naturally decomposed into an approximately low-rank structure and a sparse structure through performing LRSD. Then, the ship's wake patterns are restored in the sparse structure and detected using the RT. Biondi introduced LRSD for the first time to separate wakes and image backgrounds. LRSD is utilized both in the image and Radon domains to reduce the false alarms of the background, and then the RT is used to identify wakes [23]. In addition, there has been an extension of using LRSD in processing polarized SAR images for wake detection by using polarization information to enhance the wake features and mitigate false ship wakes [24]. On this basis, random sampling consensus was further exploited on wakes separated using LRSD to finely characterize their linear structure [25]. These existing methods have obtained success in ship detection. It has been demonstrated that the effectiveness of LRSD depends on the assumption of the high correlation of the background [26].

However, these methods mainly depend on local spatial correlations between adjacent pixels to indicate correlations, which may be corrupted by noise and significant amounts of sea clutter [26]. In fact, there are often many repetitive local patches across a whole image, which are present as nonlocal similarities [27,28]. Unlike local similarities, these

repetitive patches can be grouped together in a nonlocal matrix with high correlation to serve a low-rank structure. On the basis of this, the usage of nonlocal similarity makes a breakthrough in the application of SAR image detection and denoising. However, the existing LRSD-based ship wake methods rarely consider nonlocal similarities. On the other hand, there are also other line-shaped sea waves on the sea surface, including those induced by strong speckle noise accumulation [3,11]. These line-shaped objects are also represented as bright (dark) peak points in the Radon domain. It is difficult to distinguish between the differences in peak points between wakes and other linear structures during the threshold-based identification process [15]. As a result, the precision of wake detection is limited, and the rate of false alarms is high, especially in complex scenarios.

To address the above problems, a novel ship wake detection method based on nonlocal LRSD and an enhanced feature map for a single SAR image is proposed. First, an SAR image is divided into a grid of many image patches. To enhance the correlation, a nonlocal similarity criterion based on image entropy is employed. For each patch, a group of patches are collected based on the nonlocal entropy similarity to construct a matrix of nonlocally similar image patches, and a decomposition function is set up to modify the LRSD. Then, the FOE model is introduced to establish an enhanced feature map in order to improve the reliability of wake decisions in the nonlocal LRSD detection procedure. Finally, connected region clustering (CRC) is further executed in the Radon domain to extract the peak points of the potential wake and filter out the false points with prior knowledge of the wake breadth. Real SAR images are adopted to illustrate the effectiveness of the proposed method. The main contributions of the proposed method are as follows:

(1) Nonlocal low-rank and sparse decomposition is proposed to separate a wake from the sea background in a single SAR image. The nonlocal entropy similarity criterion is employed to measure the similarity of nonlocal image patches in a search window, and then these similar image patches are constructed as an image patch matrix to set up an objective function for LRSD.

(2) An FOE model is further introduced to improve the decision reliability of the nonlocal LRSD ship wake detection procedure. The enhanced feature map is obtained by fusing a series of multi-view feature maps, which are generated by convolution with the FOE model filters. The sparse wake obtained through nonlocal LRSD is enhanced by performing a logical "and" operation on the center points of the Radon transform results for both the sparse wake and the enhanced feature map after applying CRC to Radon images to extract central points.

The rest of this article is organized as follows. In Section 2, the principles of LRSD are overviewed, while the proposed wake detection method is presented in Section 3. The experimental results are provided in Section 4. The last section discusses the results and concludes the article.

2. LRSD for Ship Wake Detection

The redundancy and correlation in SAR images inherently stem from the repetitive nature of their internal elements. This indicates that SAR images have the properties of a low-rank structure, which is a priori knowledge in SAR images [27]. The combination of low-rank a priori knowledge of SAR images and low-rank decomposition techniques has been successfully developed in the fields of SAR image denoising and target detection [27–31]. Specifically, low-rank decomposition can be used to effectively separate low-rank background components with persistent features and sparse components representing local variations, which may correspond to targets or other objects of interest in an image, from SAR images [32]. Methods based on low-rank priors of SAR images have recently been investigated for the problem of ship detection. They assume that the stable background of SAR images exhibits a low-rank structure and approximately consider ship wake patterns, strong sea clutter, and noise as sparse components [23]. Using low-rank decomposition, the background interference can be reduced from ship wake patterns [24]. In the process, ship wake separation is formulated as an optimization problem that is

subject to the condition of sparsity [23]. The LRSD-based technique for ship wake detection unfolds in a two-step procedure: the separation of ship wake components from the background through LRSD and the detection of the wake's linear structure with the RT. The following is a brief introduction to the procedure.

A given SAR image, denoted as a two-dimensional matrix O, can be mathematically modeled as $O = L + S$, where L represents the low-rank component corresponding to the sea background, and S denotes the sparse component corresponding to the ship wake [23]. The issue of wake detection, which involves separating the ship wake from the background, is reformulated as a rank minimization optimization problem and can be approximately expressed as:

$$\min_{L,S} \|L\|_* + \lambda \|S\|_1 \quad s.t. O = L + S \tag{1}$$

where $\|\cdot\|_*$ is the nuclear norm, and $\|\cdot\|_1$ is the l_1 norm. The regularization parameter λ is used to control the balance between the two terms. The nuclear norm represents the sum of all singular values of L. The norm l_1 is the sum of the absolute values of the non-zero elements in S. Equation (1) is a convex optimization problem and is often solved using the augmented Lagrange multiplier with alternating-direction minimization [29]. The objective function is rewritten as:

$$f(L, S, Y, \mu) = \|L\|_* + \lambda \|S\|_1 + \langle Y, O - L - S \rangle + \frac{\mu}{2} \|O - L - S\|_F^2 \tag{2}$$

where $Y \in \mathbb{R}^{w \times w \times n}$ is the Lagrangian operator, μ is a positive penalty scalar, $\langle \cdot \rangle$ denotes the inner product of the matrix, and $\|\cdot\|_F$ is the Frobenius norm. Then, Equation (2) is iteratively solved for one variable by fixing the others. Taking iteration $t+1$ as an example, we update L by fixing S^t, Y^t, and μ^t:

$$\begin{aligned} L^{t+1} &= \operatorname{argmin} f\left(L, S^t, Y^t, \mu^t\right) \\ &= \|L\|_* + \lambda \left\|S^t\right\|_1 + \left\langle Y, O - L - S^t \right\rangle + \frac{\mu^t}{2} \left\|O - L - S^t\right\|_F^2 \\ &= \mathcal{U} \mathcal{S}_{\frac{1}{\mu^t}} V^T \end{aligned} \tag{3}$$

where $\mathcal{S}(\cdot)$ is a positive scale that represents a singular value-shrinkage function. Its definition is $\mathcal{S}_\varepsilon(a) = \operatorname{sgn}(a)\max(a - \varepsilon, 0)$, which is a kind of soft threshold operator, and $\operatorname{sgn}(\cdot)$ denotes the sign function. S is updated by fixing the others:

$$\begin{aligned} S^{t+1} &= \operatorname{argmin} f\left(L^{t+1}, S, Y^t, \mu^t\right) \\ &= \left\|L^{t+1}\right\|_* + \lambda \|S\|_1 + \left\langle Y, O - L - S \right\rangle + \frac{\mu^t}{2} \left\|O - L^{t+1} - S\right\|_F^2 \\ &= \mathcal{S}_{\frac{\lambda}{\mu^t}} \left(O - L^{t+1} + {Y^t}/{\mu^t} \right) \end{aligned} \tag{4}$$

where $\mathcal{S}_{\frac{\lambda}{\mu^t}}(\cdot)$ is a singular value-shrinkage function with the parameter $\frac{\lambda}{\mu^t}$. Y is updated:

$$Y^{t+1} = Y + \mu \left(O - L^{t+1} - S^{t+1} \right) \tag{5}$$

The loop procedure terminates when the maximum number of iterations is reached or the loss satisfies $\left\|O - L^t - S^t\right\|_F^2 \leq \tau$ with the error tolerance τ.

After the decomposition, the ship wake patterns are obtained in S and then detected with the RT method. The RT is applied to S to provide a Radon image R. The mean value μ_R and the standard deviation σ_R of the Radon image are estimated. A decision threshold value interval is utilized to extract the potential wake peak points, and it is expressed as $[-\mu_R - K_1 \times \sigma_R, \mu_R + K_2 \times \sigma_R]$. The parameters of K_1 and K_2 are empirically determined and conventionally set within the range of 2 to 4. These points outside the threshold interval are retained to be identified as potential wake peak points.

As shown in Equation (2), the core of analyzing low-rank priors is exploring low-rank components. For example, the background of continuous video frames involves low-rank components, since they are linearly correlated in the temporal domain [25]. The efficacy of LRSD fundamentally depends on images having low-rank properties. The more obvious the low-rank structure, the more effective the separation between the background and target, i.e., the ship wake [31]. The current LRSD-based methods for ship wake detection assume that the low-rank structure is characterized by a high correlation among adjacent pixels in an SAR image [29]. However, the correlations between neighboring pixels can be corrupted by the complexity of a scene and speckle noise [27,28]. Consequently, the performance of LRSD is confronted with this limitation, which may reduce accuracy in separating a wake from the background.

On the other hand, the success of a threshold application in the Radon domain depends on the assumption that there are distinct differences in brightness between wake components and the residual background. However, wake components are often characterized by their faint signals [33], which makes them less observable and causes differences in brightness with respect to the background to be less prominent. As a result, it is difficult to determine an appropriate threshold interval. Moreover, other linear structures, such as swell waves, also exhibit similar peak values to those of wakes in the Radon domain. Thus, this will lead to high rates of false detection alarms in the extraction of wake peak points when using a threshold decision.

3. The Proposed Method

To tackle the above problems, a novel ship wake detection method based on nonlocal LRSD and an enhanced feature map for a single SAR image is proposed. Unlike the existing LRSD method, which relies on similarity between neighboring pixels, the proposed method leverages non-local similarity in SAR images, where image patches at different spatial locations may have similar structural features [27]. Based on a predefined measurement criterion, similar image patches can be collected, and patch matrixes with a high correlation can be formed [30,31]. These nonlocal image patch matrices (NPMs) are employed to replace the original SAR images in LRSD. The entropy-based measurement criterion is also proposed to find similar image patches. As a result, the low-rank structure of an NPM is more obvious than that of the original SAR image. The separation between the wake and the background is improved by the proposed nonlocal LRSD.

In order to improve the reliability of wake decision making, it is particularly crucial to characterize the features of wake patterns. The FOE model, which has a series of high-order filters, has demonstrated its powerful ability to depict images with complex textures or structures, including edges, textures, and other high-frequency information. This model demonstrates its performance in image enhancement tasks by revealing richer and more-detailed visual details in different directions. Motivated by its characterization ability, the filters of the FOE model are introduced to generate multi-view feature maps. These maps are integrated as enhanced feature maps to support subsequent wake judgments related to sparse wakes in the Radon domain, thereby improving the reliability of decisions. Subsequently, the wake breadth is used as a filtering criterion, and CRC is performed on Radon images to extract the cluster center points of sparse wakes and enhanced feature maps. Through logical operations on the center points of their Radon images, false wakes are further removed, and the potential wake peak points are identified.

The proposed wake detection framework is overviewed in Figure 1. Initially, the SAR image is cut into a series of image patches. For each reference patch, its image entropy is calculated, and a group of patches with entropy values that are approximately the same as that of the reference patch are selected. Then, an NPM is constructed by stacking and vectorizing similar patches, and sparse wakes are separated by performing LRSD on the NPM. Secondly, the SAR image is convolved with the filters of the FOE model to obtain multi-view wake feature maps. An enhanced feature map is produced through the integration of the multi-view maps, and then low-rank matrix recovery is adopted to

reduce the noise. Finally, the RT is executed on both the sparse wake and the enhanced feature map. CRC is employed, the center points of clusters are extracted from the Radon images, and a logical "and" operation is applied on the center points to extract the peak points of the sparse wake. The wake decision results are provided by the inverse RT.

The three main steps are illustrated in detail as follows.

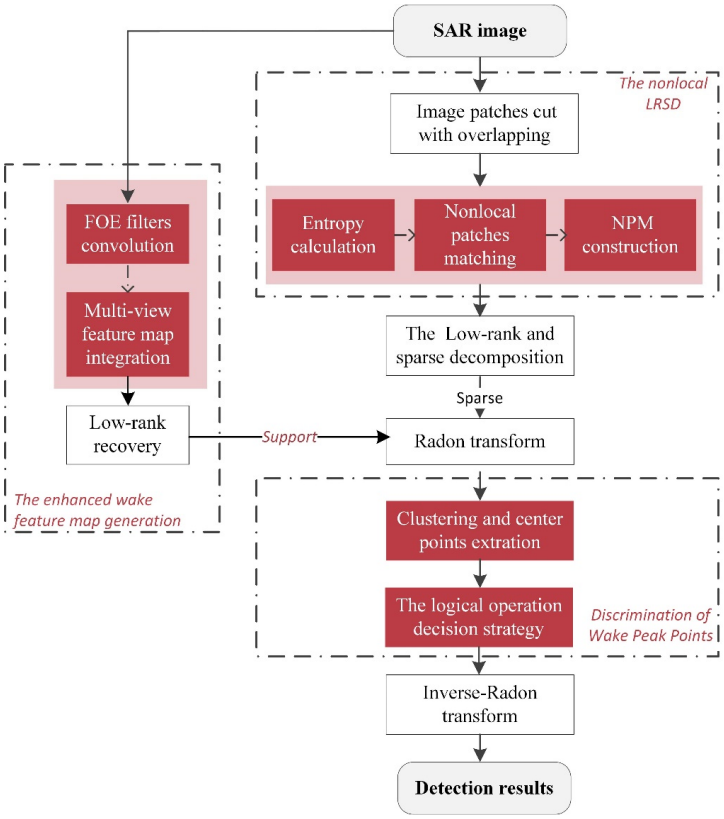

Figure 1. The outline of the proposed wake detection framework.

3.1. Modified Nonlocal LRSD

In reality, some image patches are located in different positions with similar structures. This is a typical property of SAR images and is called nonlocal similarity. Nonlocal-similarity-based methods have been investigated in SAR image denoising, restoration, and detection. These studies have demonstrated that grouped nonlocal similarity image patches can be considered as low-rank matrices. As stated previously, the successful application of LRSD depends on the low-rank structure of the SAR image. In this section, the low-rank structure of a matrix of nonlocally similar patches is exploited with similar structures, and this is incorporated into LRSD as a core concept.

Given a reference image patch, each patch can be matched with other patches according to their similarity, which is called patch matching. The key to patch matching is defining the similarity criterion. Some measurements have been adopted to evaluate the similarity of image patches, among which the most commonly adopted measurement is based on the grayscale Euclidean distance [30]. However, the large variation in the gray absolute intensity caused by noise in SAR images makes the grayscale Euclidean distance less effective. The SAR wake imaging mechanism indicates that the textural roughness of the sea surface is changed by the wake's modulation of gravity–capillary waves on the sea surface. This textural difference enables wakes to become visible in SAR images [10]. A recent study also demonstrated that wakes and the sea surface are significantly different in texture [13]. Inspired by this, texture information was utilized to assess the similarity between patches. As a classical texture feature, entropy was introduced to quantify this similarity in this study.

An SAR image with a size of $M \times N$ can be partitioned into numerous patches with a fixed size w and fixed step s. There are $((M-w+1)/s) \times ((N-w+1)/s)$ image patches. For one image patch y_i with a size of $w \times w$, the entropy is calculated as follows:

$$H_{yi} = -\sum_{m=1}^{w}\sum_{n=1}^{w} P_{m,n}\log(P_{m,n}) \tag{6}$$

where $P_{m,n} = y_i(m,n) \Big/ \sum_{m=1}^{w}\sum_{n=1}^{w} y_i(m,n)$. $y_i(m,n)$ refers to the gray intensity of y_i at (m,n). To eliminate the influence of the patch size, the entropy value is normalized as follows:

$$H_i = \frac{H_{yi}}{\log(w \times w)} \tag{7}$$

As entropy is the joint contribution of all pixels in the patch, and it is not sensitive to noise in the gray intensity [32]. The similarity criterion between the two patches can be defined using the entropy distance as follows:

$$S_{i,j} = \left|H_i - H_j\right|^2 \tag{8}$$

where H_j is the entropy of patch y_j. Then, according to the criterion in Equation (8), an NPM can be constructed for the referenced patch y_i. For each patch, the entropy of the candidate patches in a searching window is computed using Equations (7) and (8) for y_i. These candidate patches are ranked in ascending order of similarity distance. The n smallest distances are selected, and they represent the n most similar patches to the referenced patch. All of the similar patches are stretched as columns with $\mathrm{vec}(\cdot)$ and stacked to form a low-rank NPM Φ_i, where the first column denotes the referenced patch y_i. Φ_i is defined as

$$\Phi_i = [\mathrm{vec}(y_{i\_1}), \mathrm{vec}(y_{i\_2}), \ldots, \mathrm{vec}(y_{i\_n})] \tag{9}$$

where the matrix Φ_i has dimensions of $w \times w$ rows by n columns. Since the correlation between the adjacent columns in Φ_i is higher than that in the original SAR image, there are fewer sea clutter residuals in the sparse wake components. The observed image matrix O in Equation (1) is replaced by the NPM Φ_i. Similarly, a Lagrangian operator with an augmented Lagrange multiplier and alternating-direction minimization is applied to solve for each Φ_i.

An illustration of the construction of the NPM is depicted in Figure 2. The similarities among patches of ship hulls labeled with a purple box are higher than those of the surrounding sea background. The n most similar candidate patches based on the entropy similarity distance are selected, as shown in the middle of Figure 2, while the construction of Φ_i is shown on the right. The Lagrangian operator with augmented Lagrange multiplier and alternating-direction minimization is applied to solve for each Φ_i, and the whole process is summarized in Algorithm 1.

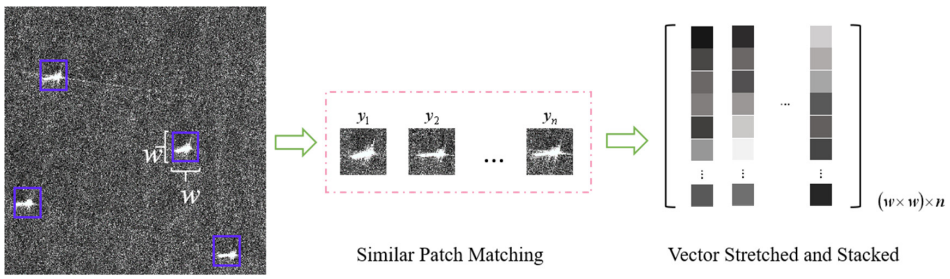

Figure 2. A schematic diagram of the construction of an NPM. The purple boxes in the grayscale SAR image on the left are similar image patches. The n most similar patches are shown in the middle; the little square on the right represents the visual pixel intensity.

Algorithm 1: Modified nonlocal LRSD based on entropy similarity

1: **Input**: An SAR image O, the maximum number of iterations T_{ita}, the tolerance τ, the size of the square patch w, and the step s between the neighboring patches.
2: Divide O into patches, find the n most similar patches, and stack the similar patch matrix Φ_i based on Equation (9); the NPM number is set to Np $\{\Phi_1, \ldots, \Phi_i, \ldots \Phi_{Np}\}$.
3: For each Φ_i in $\{\Phi_1, \ldots, \Phi_i, \ldots \Phi_{Np}\}$:
4: For $t = 1 : T_{ita}$, do the following:
5: Update L_ϕ using $US_{\frac{1}{\mu^t}}V^T$
6: Update S_ϕ using $\mathcal{S}_{\frac{\lambda}{\mu^t}}\left(\Phi - L_\phi^{t+1} + \frac{Y^t}{\mu^t}\right)$
7: Update Y using $Y^{t+1} = Y + \mu\left(\Phi - L_\phi^{t+1} - S_\phi^{t+1}\right)$
8: Update $\mu^{t+1} = \rho * \mu^t$
9: End
10: End
11: **Aggregate** L_ϕ and S_ϕ
12: **Output**

3.2. The Generation of an Enhanced Wake Feature Map

In terms of a sparse wake, it is important to enhance the linear structure characteristics, since the enhanced structure can provide supplementary information for peak point detection and improve the reliability of detection. In traditional research, regularization methods based on the weighted kernel norm and total variation (TV) are widely used to enhance the features of wakes [28]. They maintain image details by adjusting the weights of singular values or constraining the gradient information in an image. However, these methods often rely on local image priors or low-order derivative analysis factors, such as first-order derivatives, which limits their potential for describing image features. To overcome this limitation, Markov random fields (MRFs) are introduced into the detection framework, as they have shown the ability to capture image details and model spatial priors in SAR images [34]. In particular, a high-order MRF model (e.g., the FOE model) can capture global image priors through the application of a series of high-order filters [35]. These filters generate multi-view feature maps by convolving with the image and providing rich directional texture information, which is difficult to achieve with traditional methods.

Here, the high-order filters in [36] are directly employed to generate multi-view feature maps via convolution with the original SAR image, and they are written as follows:

$$f_1 = J_1^T * O, \quad f_k = J_k^T * O, \quad \ldots, \quad f_K = J_K^T * O \tag{10}$$

where J_k denotes the $k-th$ filter, which is trained with numerous natural images. f_k is the $k-th$ feature map. K is related to the number of filters, and further details can be found by referring to [36,37]. For instance, 8 filters have a size of 3×3, and 24 filters have a size of 5×5. The intricate edges and details of the images in diverse orientations are enhanced through these multi-view feature maps.

Then, an average-weighting strategy is adopted to integrate the generated feature maps into an enhanced feature map as follows:

$$F(O) = \sum_{k=1}^{K} J_k^T * O \tag{11}$$

where each feature map is assigned the same weight, since the contributions made to the feature description are the same but in different directions. The fusion process preserves the multi-view features inherent in SAR images.

Next, noise reduction is performed on the enhanced feature map by using low-rank matrix recovery.

$$\hat{O'} = \text{argmin}\frac{1}{2}\left\|F(O) - O'\right\|_2^2 + \tau\left\|O'\right\|_* \tag{12}$$

where $\hat{O}'$ is the estimated enhanced wake feature map. A singular value-shrinkage function [23] is used to solve the optimization problem in Equation (12).

To demonstrate the effectiveness of the enhanced wake feature map with the FOE model, a group of 24 filters with a size of 5×5 [37] was utilized. A content-rich GF-3 port SAR image was selected and convolved with each filter, resulting in a series of convolutional feature maps, as shown in Figure 3, where the first 24 images represented the multi-view feature maps obtained with Equation (6), and the 25th image corresponded to $\hat{O}'$. The original GF-3 port SAR image is positioned in the bottom-right corner of Figure 3. It can be observed that these multi-view feature maps encompassed rich information, and the edges were more obvious than the background. These features were highlighted through enhancement processing in various directions. In addition, the enhanced image was smoother than the original SAR image. This indicated that not only were the wake features enhanced, but the speckle noise was also reduced due to the combination of the FOE model and low-rank matrix recovery.

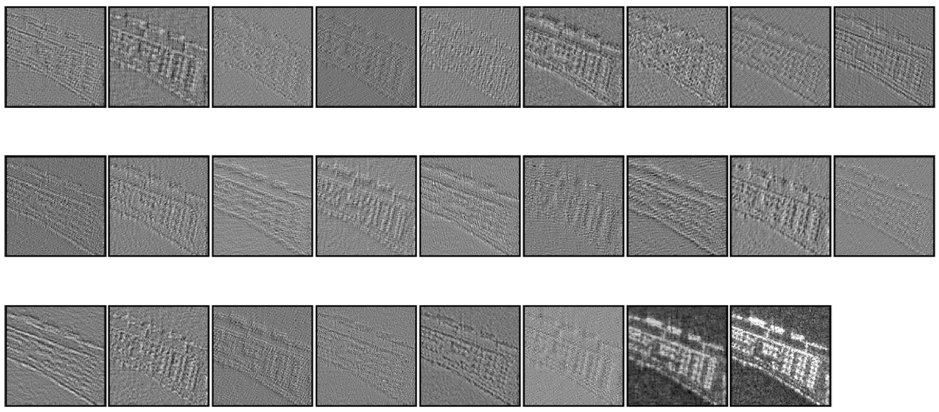

Figure 3. An illustration of generated feature maps and an SAR image.

The low-rank properties were also compared between the enhanced feature map and the original SAR image. Singular value decomposition was executed on the enhanced feature map and the original image, and the results are given in Figure 4. It can also be observed that the singular values of the feature map were smaller. As illustrated in Figure 4, the enhanced feature map had more obvious low-rank properties than those of the original SAR image. This also supported the speckle noise reduction; as such, the enhanced feature map would be beneficial for subsequent wake detection. Thus, the feature map could help separate a sparse wake from the background.

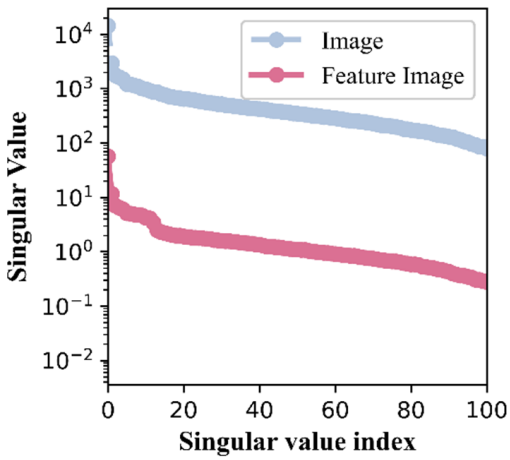

Figure 4. Comparison of the low-rank properties between an enhanced feature map and an SAR image.

3.3. Discrimination of Wake Peak Points

CRC and a logical operation are introduced to further improve the decision reliability of nonlocal LRSD in the Radon domain. Specifically, CRC is applied on both the Radon images of the sparse wake and the enhanced feature map. Based on the clustering results, a logical operation is conducted on the cluster center points.

Linear sea waves are discrete and characterized by isolated points in the Radon domain, while wake components with breadth are characterized by a contiguous region. Therefore, CRC is employed on Radon images to remove these isolated sea wave points before the logical operation.

Based on the principle of Radon-based ship wake detection, a set of peak points are retained after the threshold decision and represented by A. One peak point R_i at the location (ρ_i, θ_i) in set A is expressed as $\{\rho_i, \theta_i, I_i\}$, where ρ_i denotes the distance and θ_i denotes the angle. I_i is the brightness value of this peak. Based on the brightness of A, if all peaks have a path connecting them, then any two peaks can be considered connected. The subset composed of all peaks connected to any peak is called the connected clustering region of set A. Set A is binarized as B, and an array X_0 of the same size as B is initialized with 0. Then, the clustering regions are acquired through CRC using a structural element. The progress is expressed as follows:

$$X_t = (X_{t-1} \oplus P) \cap B \quad k = 1, 2, 3, \cdots \tag{13}$$

where P is a neighborhood structural element. The iterative process stops when $X_t = X_{t-1}$. All of the components of the connected regions are covered by X_t, and each component of the connected regions represents a set of peak points. The center point of each component of the connected regions, $\{\rho_c, \theta_c, I_c\}$ $c \in C$, is extracted gradually, where C is the total number of clustering regions.

By applying CRC to Radon images, the clustering center points are set for the sparse wake separated using nonlocal LRSD, and the enhanced feature map is obtained; these are expressed as X_{t_sw} and X_{t_ef}, respectively. Then, the potential wake peak points are extracted using a decision strategy based on a logical "and" operation, which is defined as follows:

$$X_{t\_sw}(R) \cap X_{t\_ef}(R) = \begin{cases} 1 & X_{t\_sw}(R) = X_{t\_ef}(R) = 1 \\ 0 & others \end{cases} \tag{14}$$

The ship detection results based on these potential wake peak points are provided by the inverse RT.

4. Experiments

4.1. Experimental Implementation Details

To demonstrate the performance of the proposed method, some ship wake samples from different SAR satellites were utilized for testing and comparison with other existing detection methods. The SAR image samples used for testing are depicted in Figure 5. As shown in Figure 5a–c, some ship wake data were captured by the GF-3 satellite on 31 May 2022 using the C-band frequency with a resolution of 5 m. The data in Figure 5d were obtained on 24 July 2021 with an X-band SAR sensor in the Iceye satellite with a resolution of 2.5 m. The sample in Figure 5e was acquired from open-access HRSID data and was labeled as P0137_35. In our experiments, the SAR image samples, which had a size of 196 × 196, encompassed different wake types, such as a narrow-V wake, as depicted in Figure 5. It was observed that the wake components were weak targets that were obscured by the background, making ship wake detection more difficult.

For the proposed method, the image patch size was 11 × 11, and similar image patches were collected in a search window, where $n = 90$ was used to construct the nonlocally similar patch matrix Φ with a step of $s = 5$. The iteration number was $T = 100$ for the augmented Lagrange multiplier with the alternating-direction minimized solution.

From the 24 filters illustrated in Figure 3, a subset of 9 filters was chosen to represent the wake features because of the sparsity of the multi-view feature maps. The empirical parameter within the RT was adjusted according to the SAR images. K_1 was set to 2.5, and K_2 was set to 4.

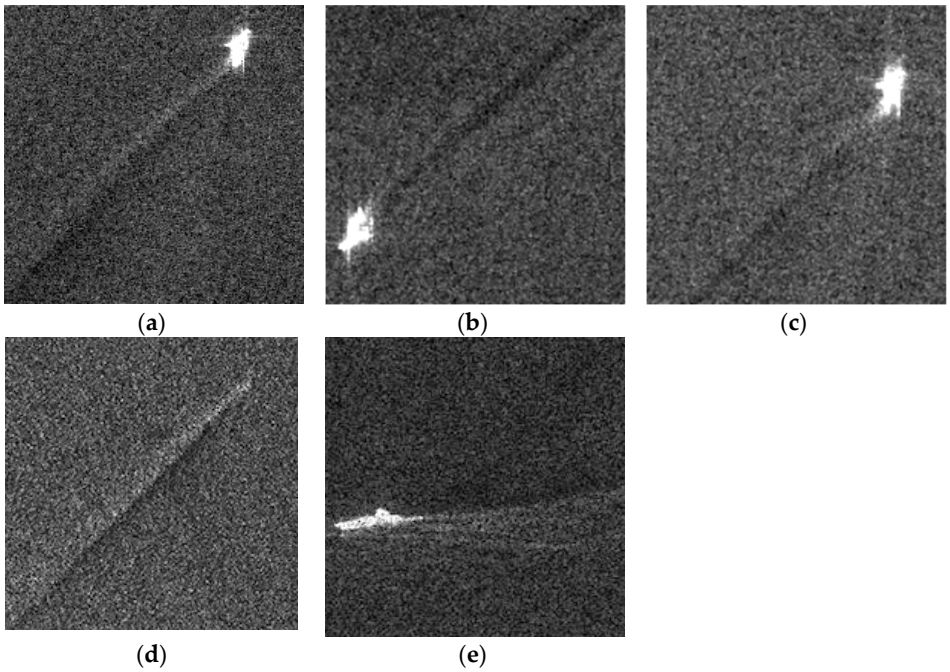

Figure 5. Experimental SAR image samples from different SAR satellites. (**a**–**c**) the GF-3 SAR images; (**d**) the SAR image sample from Iceye satellite; (**e**) SAR image sample from HRSID dataset.

4.2. Method Demonstration

First, Figure 5a is used as an example to demonstrate the experimental process in detail. As depicted in the flowchart in Figure 1, the entire experiment was divided into three main stages: the implementation of NLRSD, the enhancement of wake features, and wake peak discrimination using clustering in the Radon transform domain. For convenience, NLRSD and EFM are used as shorthand for the proposed nonlocal LRSD and the enhanced feature map, respectively.

The SAR image in Figure 5a was broken down into low-rank components, as shown in Figure 6a, and a sparse wake, as shown in Figure 6b, by using NLRSD as described in Section 3.1. It was observed that the sparse wake components shown in Figure 6b were more visible than in the original image. This revealed the effect of ship wake separation based on NLRSD, which aimed to improve the observability of ship wake patterns against the background. As shown in Figure 6b, it was also found that the boundaries of the separated wake still seemed to be as blurry as those in the original. These blurry boundaries would lead to weak distinguishability between wake peak points and the background in the Radon domain, thereby increasing the risk of false alarms. As such, it was necessary to enhance the wake edge features to improve the peak decision making.

In accordance with Section 3.2, an enhanced feature map for Figure 5a was generated, as shown in Figure 6c. It can be seen that the wake and its edges were more distinct than those in the sparse wake and the original SAR image. This indicated that the proposed enhanced feature maps possessed the ability to characterize and amplify the linear structures of wakes.

Then, based on the processed results, the potential wake peak extraction in the Radon transform domain was subsequently demonstrated. The outputs of the separated sparse ship wake and the enhanced feature map were subjected to the Radon domain. CRC was then performed within the two Radon outputs, and the centroids of these clustering results from both Radon outputs were combined through logical operations to yield potential wake

peak judgment points. Figure 7a shows the Radon output of the sparse wake, and Figure 7b shows the clustering center point distribution in the Radon output. Correspondingly, the Radon output and clustering center points for the enhanced feature map are displayed in Figure 7c,d. The output for the extracted potential wake peak point is shown in Figure 7e.

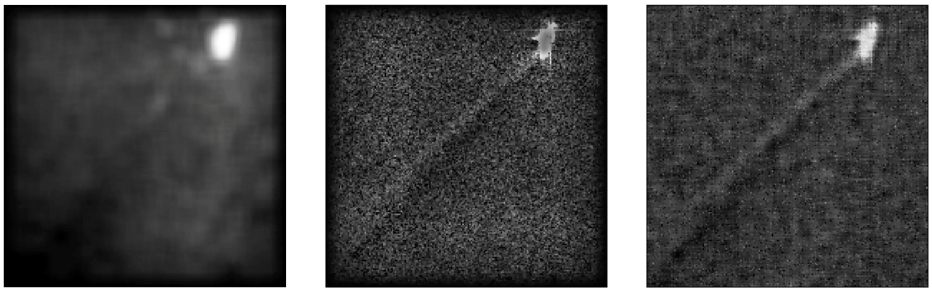

(**a**) (**b**) (**c**)

Figure 6. The decomposition and enhanced feature map results for Figure 5a. From left to right: (**a**) the low-rank component; (**b**) the sparse wake; and (**c**) the enhanced feature map, respectively.

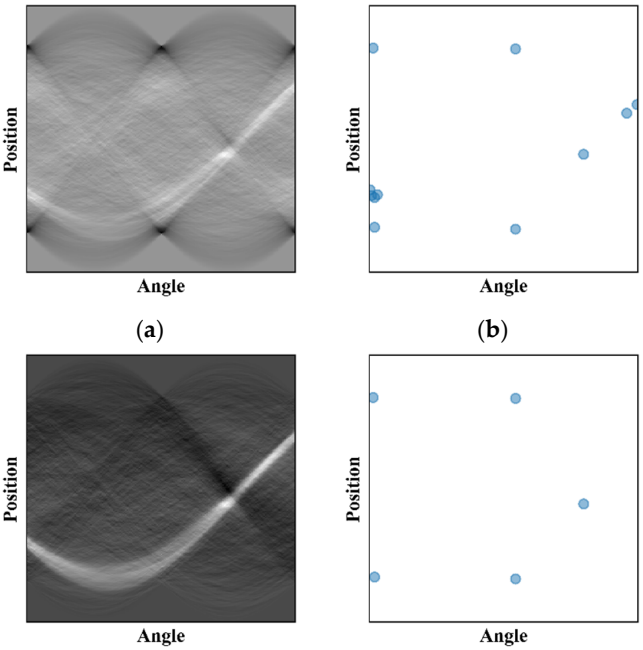

Figure 7. The Radon output and its clustering center point distribution. (**a**) The Radon outcome for the sparse wake; (**b**) center point distribution of (**a**); (**c**) Radon outcome for the enhanced feature map; (**d**) center point distribution of (**c**); (**e**) the extracted potential wake peak point.

Obviously, the Radon output of the sparse wake in Figure 7a was smoother than that of the enhanced feature map in Figure 7c, which suggested the effect of NLRSD on the reduction in the background interference and indicated the advantage of this methodology. The heightened luminance contrast between peak points in the Radon output derived from the enhanced feature map confirmed the potency of the feature enhancement methodology. This afforded a clearer visual representation for wake identification, as shown in Figure 6.

The clustering center points were obtained by clustering the Radon output, so the distribution of the center points could reflect the distribution of lines in the images. For example, if only one point existed in the clustering, there would only be one line in the image. This was also observed in the presence of a few center points in Figure 7b, which indicated a potential limitation in the precision of wake detection afforded by NLRSD. Observation of Figure 7e suggests that the incorporation of an enhanced feature map into NLRSD in the Radon domain presents a potential way to augment the precision and reliability of wake recognition.

4.3. Contrastive Experimental Results

Finally, to illustrate the efficacy of the proposed method, its detection performance on the real SAR image samples shown in Figure 5 was compared with that of existing methods, including LRSD [23], GMC [15], a wavelet-transform-based method [19], and the fast Radon method [14]. GMC is a state-of-the-art wake detection method. Specifically, the detection results and the computational complexity of execution were analyzed and compared. To ensure consistency in the experimental conditions, CRC was also applied to the compared methods.

The detection results of the five methods are shown in Figures 8–12. The results of the fast Radon method failed to achieve satisfactory accuracy, with many false alarms being observable. As a classical wake detection method, this was attributed to it rarely considering the suppression of background interference. In the results of the wavelet- and LRSD-based methods, the false-alarm rate was reduced compared with that of the fast Radon method. The visual results indicate that the accuracy of LRSD was better than that of the wavelet-based method, which suggested the effectiveness of low-rank-based detection methods for wake detection. As shown in Figure 9, the GMC method outperformed the other three methods used for comparison and could sometimes achieve a detection accuracy comparable to that of the proposed method. As shown in Figure 11, its accuracy was even slightly higher than that of the proposed method. However, it is regrettable that it occasionally exhibited missed detections, as seen in Figure 12. In contrast, the proposed method yielded satisfactory results. The detection precision of the method introduced in this study was generally higher than that of the methods used for comparison, and the effect of eliminating false positives was also relatively competitive. This also illustrated that the nonlocal method proposed in this study could be used to construct a matrix with higher correlations to effectively reduce the background interference, while incorporating the enhanced feature map improved the reliability of ship wake judgment, thereby filtering out the probability of false alarms. The application proved the reliability of the proposed method in practice.

Additionally, we conducted a statistical analysis of the time consumed by the different methods during their execution. The average execution time of the methods on the sample images was counted, and the results are listed in Table 1. In comparison with the existing methods, our approach incurred more computational time. The extended computational duration associated with our proposed algorithm was mainly attributed to the requirement of constructing nonlocal image patch matrices, which could improve the detection performance. For each matrix, repetitive calculations of image entropy and low-rank singular value decomposition (SVD) were required. Consequently, this resulted in a longer time commitment than that of the existing methods. Although this process required more time, the resultant enhancement in performance was evident.

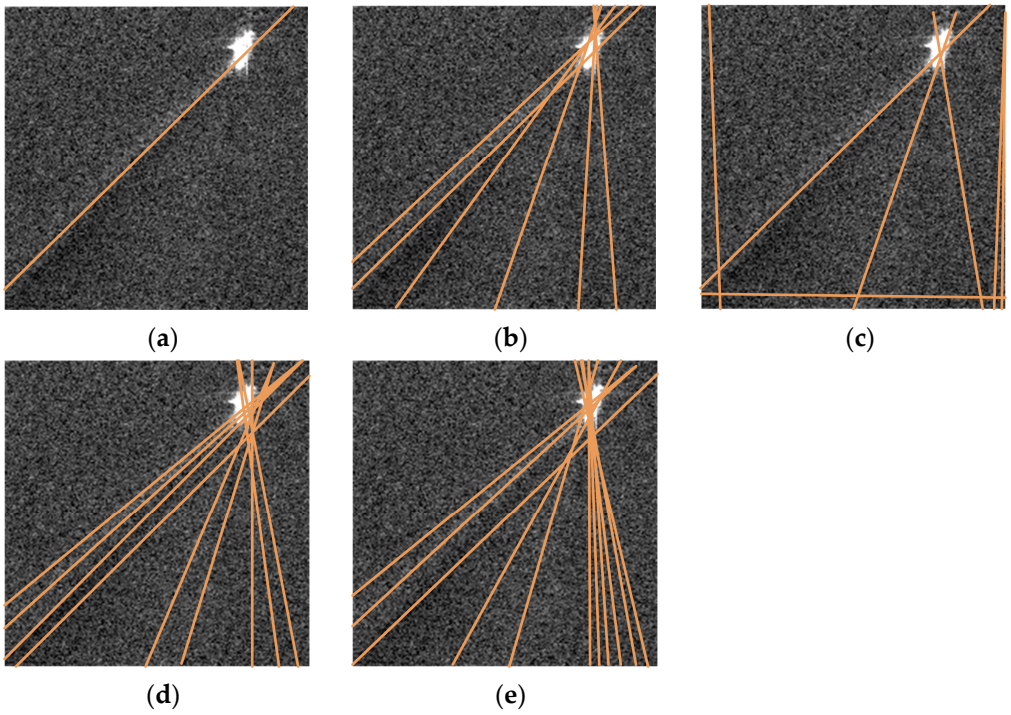

Figure 8. Comparison of the results of ship wake detection in sample images in Figure 5a with different methods. (**a**) Proposed method; (**b**) LRSD; (**c**) GMC; (**d**) wavelet-based method; (**e**) fast Radon method.

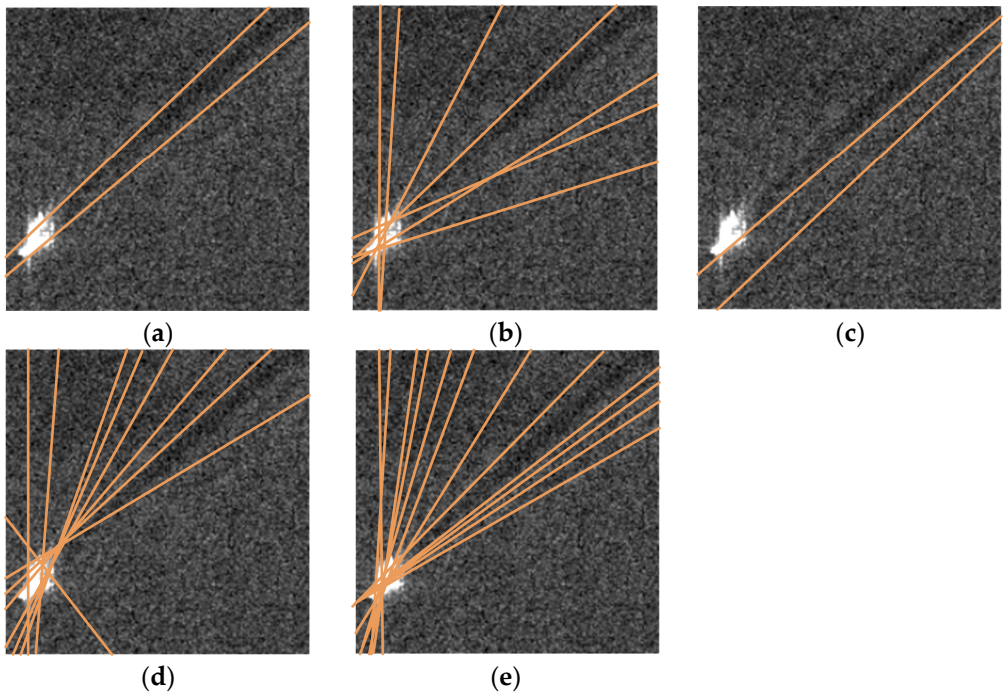

Figure 9. Comparison of the results of ship wake detection in sample images in Figure 5b with different methods. (**a**) Proposed method; (**b**) LRSD; (**c**) GMC; (**d**) wavelet-based method; (**e**) fast Radon method.

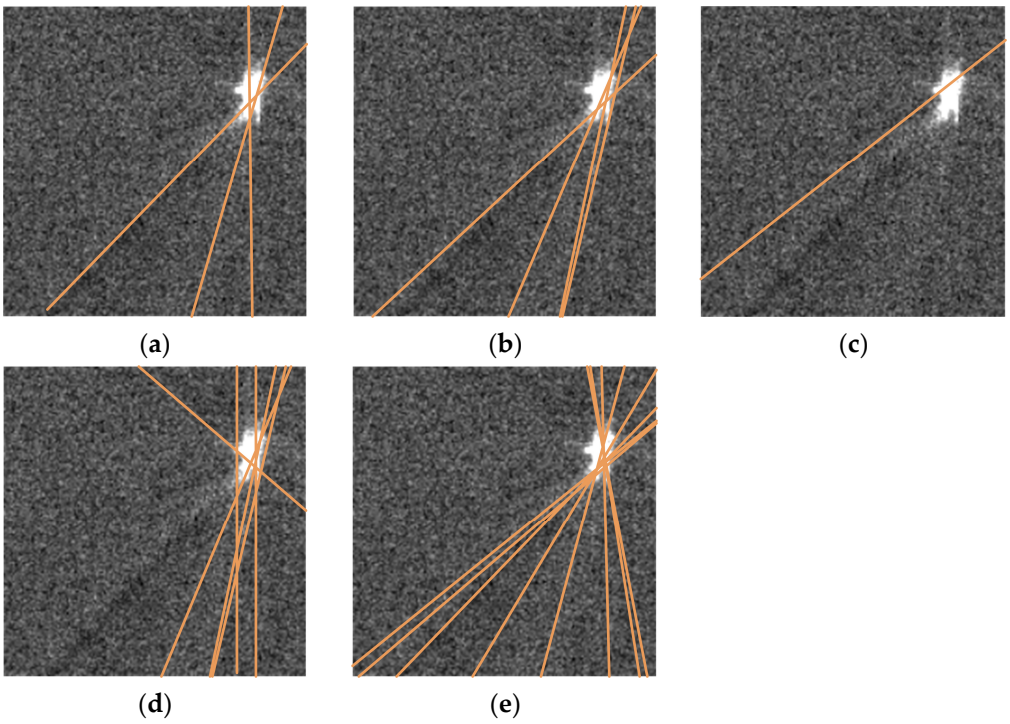

Figure 10. Comparison of the results of ship wake detection in sample images in Figure 5c with different methods. (**a**) Proposed method; (**b**) LRSD; (**c**) GMC; (**d**) wavelet-based method; (**e**) fast Radon method.

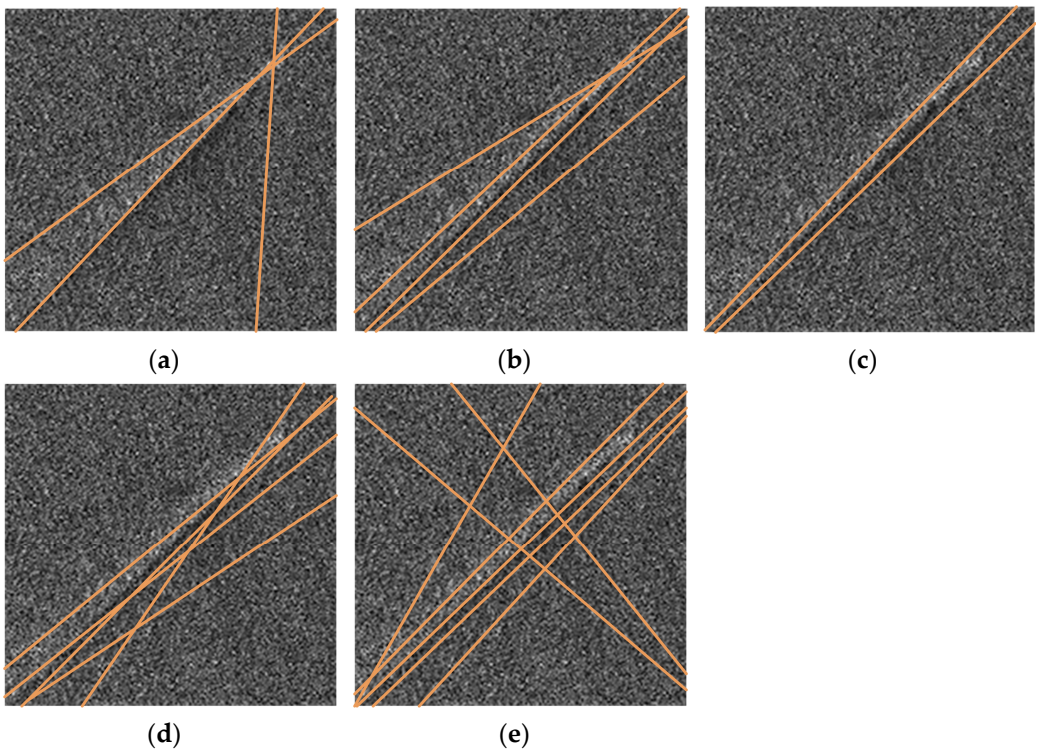

Figure 11. Comparison of the results of ship wake detection in sample images in Figure 5d with different methods. (**a**) Proposed method; (**b**) LRSD; (**c**) GMC; (**d**) wavelet-based method; (**e**) fast Radon method.

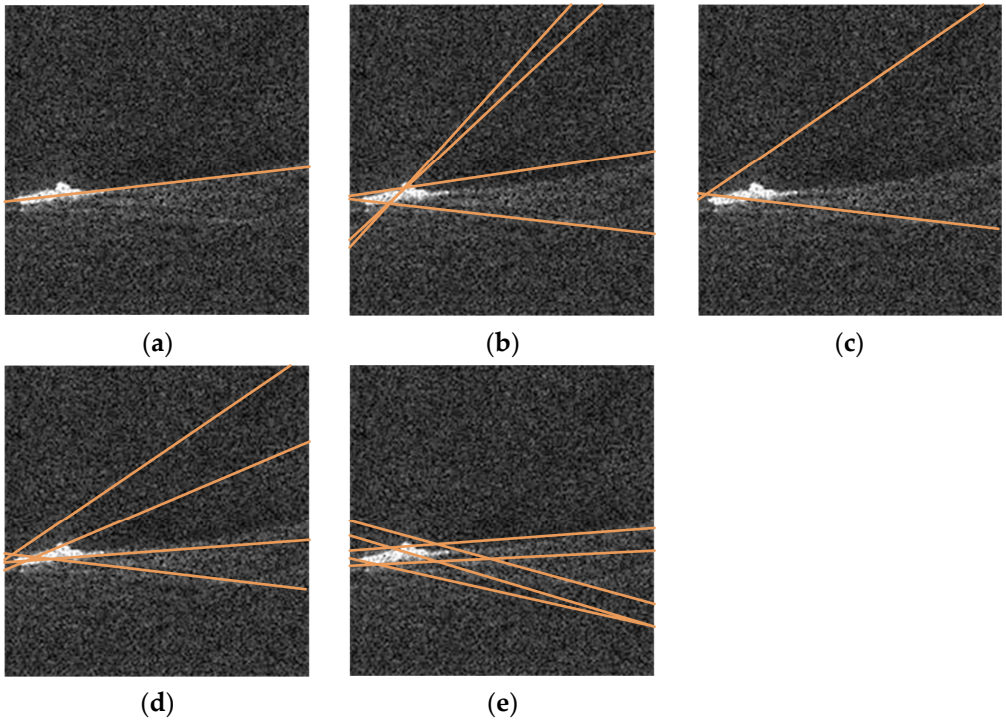

Figure 12. Comparison of the results of ship wake detection in sample images in Figure 5e by using different methods. (**a**) Proposed method; (**b**) LRSD; (**c**) GMC; (**d**) wavelet-based method; (**e**) fast Radon method.

Table 1. Comparison of the execution time (s).

	NLRSD	LRSD	GMC	Wavelet-Based Method	Fast Radon Method
Time	810	25	450	18	13

5. Discussion and Conclusions

This study was motivated by the objective of increasing the accuracy of ship wake detection in SAR images and decreasing the rate of false alarms. Conventional LRSD-based studies have primarily focused on background removal, ignoring the nonlocal similarity priors and the reliability of wake decision making. This investigation indicated that wake separation can be improved by using modified nonlocal LRSD. Enhanced wake features can serve to distinguish between the true linear structure of a wake and the other false structures. An analysis of the results for the computational time in a comparison between NLSD and LRSD was also provided. There are two primary complex computations in the proposed method. The first involves the decomposition process of singular value decomposition (SVD), a fundamental component of LRSD-based methods. The computational complexity of constructing an NPM is $O(w^2 \times n^2)$, according to the parameters set in the experiment. The SVD is executed T times in a loop, and the complexity is $T \times O(w^2 \times n^2)$. The other is the calculation of entropy, for which the computational complexity of one patch is calculated as $O(w^2)$. As described in Section 3.1, the computation of entropy necessitates repetitive evaluations for each image patch. Moreover, the calculation of entropy is iteratively executed within all candidate patches, thereby augmenting the computational burden. The improvement of the detection accuracy is at the cost of computational complexity, and future work will focus on reducing the runtime of the method while maintaining high detection accuracy.

A novel ship wake detection procedure based on a nonlocal low-rank constraint and an enhanced feature map was proposed in order to improve the reliability of wake decisions.

The designed nonlocal similarity criterion was utilized to construct a matrix of nonlocally similar image patches with high correlation, which provided a better separation between sea clutter and wake patterns. An enhanced feature map was developed using the FOE model to capture more wake details, thereby improving the reliability of wake peak point decisions. Based on Radon images, clustering in connection regions was further employed to filter out other linear structures of sea waves and noise. Our method demonstrated remarkable detection accuracy when applied to real SAR images. However, it is worth noting that the proposed method incurs higher computational costs due to the construction of a nonlocally similar patch matrix. The trade-off between accuracy and computational efficiency is a challenge that must be addressed in future research.

Author Contributions: Conceptualization, Y.G., H.X. and C.L.; methodology, Y.G. and H.X.; software, Y.G.; validation, Y.G. and H.X.; formal analysis, H.X. and W.L.; investigation, Y.G.; data curation, H.X.; writing—original draft, Y.G.; writing—review and editing, H.X. and C.L. supervision, H.X., W.L. and C.L. All authors have read and agreed to the published version of the manuscript.

Funding: This research was funded by National Natural Science Foundation of China (U2241202) and National Key R&D Program of China (2022YFB3902300).

Data Availability Statement: The data presented in this study are available upon request from the corresponding author.

Conflicts of Interest: The authors declare no conflicts of interest.

References

1. Wang, Y.; Wang, C.; Zhang, H.; Dong, Y.; Wei, S. A SAR Dataset of Ship Detection for Deep Learning under Complex Backgrounds. *Remote Sens.* **2019**, *11*, 765. [CrossRef]
2. Graziano, M.D.; D'Errico, M.; Rufino, G. Ship heading and velocity analysis by wake detection in SAR images. *Acta Astronaut.* **2016**, *128*, 72–82. [CrossRef]
3. Zilman, G.; Zapolski, A.; Marom, M. The speed and beam of a ship from its wake's SAR images. *IEEE Trans. Geosci. Remote Sens.* **2004**, *42*, 2335–2343. [CrossRef]
4. Li, J.; Wang, L.; Zhang, M.; Jiao, Y.-C.; Liu, G. Ship Velocity Automatic Estimation Method Via Two-Dimensional Spectrum Pattern of Kelvin Wakes in SAR Images. *IEEE J. Sel. Top. Appl. Earth Obs. Remote Sens.* **2021**, *14*, 4779–4786. [CrossRef]
5. Grosso, E.; Guida, R. A New Automated Ship Wake Detector for Small and Go-Fast Ships in Sentinel-1 Imagery. *Remote Sens.* **2022**, *14*, 6223. [CrossRef]
6. Ren, W.J.; Liu, P.; Ren, X.-C.; Jin, Y.-Q. SAR Image Simulation of Ship Turbulent Wake Using Semi-Empirical Energy Spectrum. *IEEE J. Multiscale Multiphys. Comput. Tech.* **2021**, *6*, 1–7. [CrossRef]
7. Graziano, M.D. Preliminary Results of Ship Detection Technique by Wake Pattern Recognition in SAR Images. *Remote Sens.* **2020**, *12*, 2869. [CrossRef]
8. Fujimura, A.; Soloviev, A.; Kudryavtsev, V. Numerical Simulation of the Wind-Stress Effect on SAR Imagery of Far Wakes of Ships. *IEEE Geosci. Remote Sens. Lett.* **2010**, *7*, 646–649. [CrossRef]
9. Liu, Y.; Zhao, J.; Qin, Y. A novel technique for ship wake detection from optical images. *Remote Sens. Environ.* **2021**, *258*, 112375. [CrossRef]
10. Xue, F.; Jin, W.; Qiu, S.; Yang, J. Rethinking Automatic Ship Wake Detection: State-of-the-Art CNN-Based Wake Detection via Optical Images. *IEEE Trans. Geosci. Remote Sens.* **2022**, *60*, 5613622. [CrossRef]
11. Courmontagne, P. An improvement of ship wake detection based on the radon transform. *Signal Process.* **2005**, *85*, 1634–1654. [CrossRef]
12. Copeland, A.C.; Ravichandran, G.; Trivedi, M.M. Localized Radon Transform-Based Detection of Ship Wakes in SAR Images. *IEEE Trans. Geosci. Remote Sens.* **1995**, *33*, 35–45. [CrossRef]
13. Guan, Y.; Xu, H.; Liu, W.; Li, C.; Liu, Y. A False-Alarm-Controllable Modified AdaBoost Wake Detection Method Using SAR Images. *IEEE Sens. J.* **2023**, *23*, 29394–29405. [CrossRef]
14. Zilman, G.; Zapolski, A.; Marom, M. On Detectability of a Ship's Kelvin Wake in Simulated SAR Images of Rough Sea Surface. *IEEE Trans. Geosci. Remote Sens.* **2015**, *53*, 609–619. [CrossRef]
15. Karaku¸s, O.; Rizaev, I.; Achim, A. Ship Wake Detection in SAR Images via Sparse Regularization. *IEEE Trans. Geosci. Remote Sens.* **2020**, *58*, 1665–1677. [CrossRef]
16. Graziano, M.D.; D'Errico, M.; Rufino, G. Wake component detection in X-band SAR images for ship heading and velocity estimation. *Remote Sens.* **2016**, *8*, 498. [CrossRef]
17. Murphy, L.M. Linear Feature Detection and Enhancement in Noisy Images via the Radon Transform. *Pattern Recognit. Lett.* **1986**, *4*, 279–284. [CrossRef]

18. Rey, M.T.; Tunaley, J.K.; Folinsbee, J.T.; Jahans, P.A.; Dixon, J.A.; Vant, M.R. Application of Radon Transform Techniques to Wake Detection in Seasat-A SAR Images. *IEEE Trans. Geosci. Remote Sens.* **1990**, *28*, 553–560. [CrossRef]
19. Jin, M.K.; Chen, K.S. The application of wavelets correlator for ship wake detection in SAR images. *IEEE Trans. Geosci. Remote Sens.* **2003**, *41*, 1506–1511. [CrossRef]
20. Arnold-Bos, A.; Martin, A.; Khenchaf, A. Obtaining A Ships Speed and Direction from Its Kelvin Wake Spectrum Using Stochastic Matched Filtering. In Proceedings of the IEEE International Geoscience and Remote Sensing Symposium, Barcelona, Spain, 23–28 July 2007; pp. 1106–1109.
21. Kang, K.M.; Kim, D.J. Ship Velocity Estimation From Ship Wakes Detected Using Convolutional Neural Networks. *IEEE J. Sel. Top. Appl. Earth Obs. Remote Sens.* **2019**, *12*, 4379–4388. [CrossRef]
22. Yang, G.; Yu, J.; Xiao, C.; Sun, W. Ship Wake Detection for SAR Images with Complex Backgrounds Based on Morphological Dictionary Learning. In Proceedings of the 2016 IEEE International Conference on Acoustics, Speech and Signal Processing (ICASSP), Shanghai, China, 20–25 March 2016; pp. 1896–1900.
23. Biondi, F. Low-rank plus sparse decomposition and localized radon transform for ship-wake detection in synthetic aperture radar images. *IEEE Geosci. Remote Sens. Lett.* **2018**, *15*, 117–121. [CrossRef]
24. Biondi, F. A Polarimetric Extension of Low-Rank Plus Sparse Decomposition and Radon Transform for Ship Wake Detection in Synthetic Aperture Radar Images. *IEEE Geosci. Remote Sens. Lett.* **2019**, *16*, 75–79. [CrossRef]
25. Zhao, Y.H.; Han, X.; Liu, P. A RPCA and RANSAC Based Algorithm for Ship Wake Detection in SAR Images. In Proceedings of the 2018 12th International Symposium on Antennas, Propagation and EM Theory (ISAPE), Hangzhou, China, 3–6 December 2018; IEEE: Piscataway, NJ, USA, 2018; pp. 1–4.
26. Guan, D.; Xiang, D.; Tang, X.; Kuang, G. SAR Image Despeckling Based on Nonlocal Low-Rank Regularization. *IEEE Trans. Geosci. Remote Sens.* **2019**, *57*, 3472–3489. [CrossRef]
27. Vitale, S.; Cozzolino, D.; Scarpa, G.; Verdoliva, L.; Poggi, G. Guided Patchwise Nonlocal SAR Despeckling. *IEEE Trans. Geosci. Remote Sens.* **2019**, *57*, 6484–6498. [CrossRef]
28. Chen, G.; Li, G.; Liu, Y.; Zhang, X.P.; Zhang, L. SAR Image Despeckling Based on Combination of Fractional-Order Total Variation and Nonlocal Low Rank Regularization. *IEEE Trans. Geosci. Remote Sens.* **2020**, *58*, 2056–2070. [CrossRef]
29. Guo, Y.; Liao, G.; Li, J.; Gu, T. Clutter Suppression Method Based on NSS-RPCA in Heterogeneous Environments for SAR-GMTI. *IEEE Trans. Geosci. Remote Sens.* **2020**, *58*, 5880–5891. [CrossRef]
30. Bo, F.; Lu, W.; Wang, G.; Zhou, M.; Wang, Q.; Fang, J. A Blind SAR Image Despeckling Method Based on Improved Weighted Nuclear Norm Minimization. *IEEE Geosci. Remote Sens. Lett.* **2022**, *19*, 4515305. [CrossRef]
31. Leibovich, M.; Papanicolaou, G.; Tsogka, C. Low Rank Plus Sparse Decomposition of Synthetic Aperture Radar Data for Target Imaging. *IEEE Trans. Comput. Imaging* **2020**, *6*, 491–502. [CrossRef]
32. Sun, Y.; Lei, L.; Guan, D.; Li, X.; Kuang, G. SAR Image Change Detection Based on Nonlocal Low-Rank Model and Two-Level Clustering. *IEEE J. Sel. Top. Appl. Earth Obs. Remote Sens.* **2020**, *13*, 293–306. [CrossRef]
33. Graziano, M.; Grasso, M.; D'Errico, M. Performance Analysis of Ship Wake Detection on Sentinel-1 SAR Images. *Remote Sens.* **2017**, *9*, 1107. [CrossRef]
34. Zhang, P.; Li, M.; Wu, Y.; An, L.; Jia, L. Unsupervised SAR image segmentation using high-order conditional random fields model based on product-of-experts. *Pattern Recognit. Lett.* **2016**, *78*, 48–55. [CrossRef]
35. Xiong, B.; Liu, Q.; Xiong, J.; Li, S.; Wang, S.; Liang, D. Field-of-Experts Filters Guided Tensor Completion. *IEEE Trans. Multimed.* **2018**, *20*, 2316–2329. [CrossRef]
36. Roth, S.; Black, M.J. Fields of Experts: A Framework for Learning Image Priors. *Proc. IEEE Comput. Soc. Conf. Comput. Vis. Pattern Recognit.* **2005**, *2*, 860–867.
37. Roth, S.; Black, M.J. Fields of Experts. *Int. J. Comput. Vis.* **2009**, *82*, 205–229. [CrossRef]